

Signatures of Wannier-Stark and surface states in electron tunneling and related phenomena: Electron transmission through a tilted band

Alexander Onipko and Lyuba Malysheva[†]

Department of Physics, Uppsala University, Box 530, S-751 21 Uppsala, Sweden

**Department of Physics, IFM, Linköping University, S-581 83 Linköping, Sweden*

[†]Bogolyubov Institute for Theoretical Physics, Kiev, 03143, Ukraine

(November 5, 2018)

Predicted by Wannier in 1960 band states quantization in a constant electric field, $E_n = \text{const} \pm n\mathcal{E}$, where $n = 0, 1, 2, \dots$, and \mathcal{E} is proportional to the strength of electric field [this kind of spectrum is commonly referred as the Wannier-Stark ladder (WSL)], implies that the probability of tunneling through a tilted band should have \mathcal{E} spaced peaks, at least, under the weak coupling of the band states to the source and drain electrodes. It has been shown, however, (Phys. Rev. B **63**, ..., 2001), that the appearance of the canonical WSL is preceded by WSLs with other level spacing, namely, $\mathcal{E}_{m'/m}/(1-2m'/m)$, where m and $m' < m/2$ are positive integers specifying certain applied voltage. Here we show that canonical and noncanonical WSLs, in addition to different peak spacing in the transmission spectrum, have other pronouncedly distinctive features. As an example, for the former, the peak and valley tunneling probability decays exponentially with the increase of applied voltage. The corresponding exponents are given by the sum and difference of two Fowler-Nordheim-type exponents implying an anomalous increase of the peak-to-valley ratio. These and other signatures of extended states (es), surface localized states (sls), and Wannier-Stark (WS) states in the through tilted band transmission spectrum are discussed on the basis of (derived for the first time) nearly exact explicit expressions of es-, sls-, and WS states assisted tunneling probability.

^{*}Also the address for communication

I. INTRODUCTION

Introduced by Wannier in 1960,^{1,2} the concept of Wannier-Stark ladder (WSL), associated with the spectrum of electron band states in a constant electric field, gave rise to an unobservable literature of discussions aimed at the development of in-depth understanding of electric field effects in solids. In nineties, this activity has resulted in several reports on experimental observation of the Wannier-Stark (WS) effect, Bloch oscillations, and related coherent phenomena,^{3–5} appearance of new ideas (such as, e.g., dynamic localization⁶ and quasi-energy band collapse in time-dependent electric fields,^{7–9}) and new possibilities to study static and time dependent field effects in optically driven lattices.^{10–15}

In its canonical form, the WSL represents a spectrum of evenly spaced electronic levels $E_n = \text{const} \pm n\mathcal{E}$, where $n = 0, 1, 2, \dots$, and \mathcal{E} (the level spacing proportional to the strength of electric field) is equal to the Plank constant times Bloch oscillation frequency. In the tight-binding description, this kind of spectrum is readily expected,¹⁶ if the constant shift \mathcal{E} of electron on-site (atomic) energy along the electric field is comparable with the width of the parent zero-field band of Bloch electron states. Such an extreme case of WSL, though is easy to think about, is of little, if any, physical interest, since in most cases, the band state spectrum emerges as a result of delicate interplay of electric field and interatomic interaction effects, where the methodology of perturbation theory is inappropriate.

In early seventies, it was realized that the tight-binding model presents a unique opportunity to treat field effects in solids on rigorous basis, since its Hamiltonian admits obtaining the exact formal solution of the Schrödinger equation^{17–20} and hence, the Green function problem,^{21–23} without any restriction on the field parameter. A number of useful results has been obtained in this way,^{17–19,22–24} in particular, that in finite systems, some minimal voltage is required to open the WS band.¹⁹ Unlike the Wannier model, which refers to the bulk electron states only, the field-induced surface states also have been brought to light. It was shown that eigenenergies near the spectrum edges behave similarly to zeros of the Airy function.^{18,19,24} Recently,²⁵ within the same model, new regularities for the bulk and surface electron states influenced by a constant electric field were predicted. The bulk levels, for instance, have been shown to form (under certain voltages) WSLs with noncanonical level spacing $q\mathcal{E}$, where $q (> 1)$ can be an integer, as well as a fractional number. Thus the concept of WSL appeared even more rich and fertile physically, than was commonly thought.

Next step to be undertaken is to specify such physical quantities, which allow one to observe distinctions between the true Wannier levels and the others, for instance, the levels that correspond to *extended states* (es) and form noncanonical WSLs, and those corresponding to *surface localized states* (sls), whose spacing is governed by three different laws.²⁵ Here, in focus is the probability of tunneling (or transmission) of electrons through a tilted tight-binding band. This quantity is of relevance to the phenomenon of electrical breakdown of ultra-thin dielectric layers and a number of other electric field effects in solids. The energy dependence of electron transmission can be directly probed by means of the ballistic-electron-emission microscopy technique.²⁶ And properties of through tilted band tunneling are intimately related to Zener tunneling and Franz-Keldysh effect.

II. MODEL AND GENERAL CONSIDERATION

We choose to discuss the electric field effects on tunneling through a spatially finite and energetically restricted band of electronic states in the context of electron ballistic transport in superlattices. The profile of \mathcal{N} -well superlattice model potential is shown by dashed line in Fig. 1. Due to electron confinement in a well, the well spectrum is quantized. Due to tunneling between neighboring wells, the quasi-discrete (in its lower part) spectrum of an isolated well splits into minibands of allowed electron energies, separated by the energy gaps, which do not contain electron states. Since the height and width of barriers can be engineered freely within a wide range, it is well possible to have the lowest miniband separated from the others by an energy interval much exceeding its band width E_{bw} . An example of this kind is represented in Fig. 1.

Under a restriction that the electrostatic potential drop across the superlattice does not exceed much the magnitude of E_{bw} , the description of electron transport along the superlattice can be started from the Hamiltonian matrix for a single band

$$H_{nn'} = \mathcal{E} [n - (\mathcal{N} + 1)/2] \delta_{n,n'} + \delta_{|n-n'|,1}, \quad (1)$$

where indices $n, n' = \overline{1, \mathcal{N}}$ number the wells in the superlattice (see Fig. 1); $\mathcal{E} = eFa/\beta$; e , F , and a are, respectively, the absolute value of electron charge, electric field strength, and periodicity of the superlattice $a = w_w + w_b$; the energy of electron resonance transfer between neighboring wells β serves as an energy unit; the zero-field energy of the lowest level in the non-interacting wells (the electron on-site energy) is set equal to zero.

The eigenvalues of the Hamiltonian matrix (1) are lying within the (dimensionless) energy interval (along E axis in Fig. 1) which is equal to $E_{\text{bw}} + eV$, $E_{\text{bw}} = 4$, $eV = \mathcal{E}(\mathcal{N} - 1)$. Excluding classically inaccessible regions in the n - E 'coordinates', one obtains a tilted band of electron states. Such a band is shown in Fig. 1 for two voltages $eV < E_{\text{bw}}$ and $eV > E_{\text{bw}}$. Sloped lines on the band diagrams indicate the n - E (unshaded) regions, where the probability to find an electron with the given energy in a well n ($= 1, 2, \dots, \mathcal{N}$) is proportional to the tailing part of the corresponding squared eigenfunction of $H_{nn'}$. As is seen from the figure, if the applied potential is smaller, than the miniband width in zero field, $eV < E_{\text{bw}}$, the band spectrum can be divided into es-band and two sls-bands; at higher voltages $eV > E_{\text{bw}}$, the es-band is replaced by WS-band.

Let us assume that from its opposite boundary layers, the superlattice is contacted homogeneously to ideal semi-infinite drain and source electrodes and, that the interaction between its first (\mathcal{N} th) well and the drain (source) lead can be described by a single parameter \mathcal{V} . According to the model, the electrostatic potential energy inside the leads is constant (though different) and drops from the source to drain by value of eV , entirely in the region occupied by the superlattice, see energy diagrams in Fig. 2. Suppose also that the spatial variables of the Hamiltonian of the system drain-superlattice-source are separable. Then, the electron energy E can be broken into a sum of two non-mixing components which correspond to the energy of electron motion parallel (E_{\parallel}) and perpendicular (E_{\perp}) to the electric field, the latter directed along the superlattice. In such a system, an electron wave, having the energy E and propagating freely, say, in the source towards the drain, will be transmitted through the superlattice with the probability $T(E, \mathcal{E})$. Due to the Landauer-Büttiker theory,^{27–29} the transmission probability is directly related to the current-voltage relation, see, e.g., the Datta overview.³⁰

Probably, for the first time, the model of ballistic electron transport outlined above was suggested and solved on the basis of the Green function technique by Caroli *et al.*³¹ Originally, it was applied to the description of tunnel current in metal-insulator-metal heterostructures. To calculate the current, the Green function has to be found. In the cited work, however, the latter was not specified. Later on, the variations of Caroli *et al.* treatment have reemerged in a number of physical contexts. In particular, it has been used to examine the quantum conductance of molecular wires.^{32–34}

For the model at hand, the transmission probability $T(E, \mathcal{E})$ is conveniently expressible in terms of certain matrix elements of the Green functions referred to the *non-interacting* source and drain leads, and the scattering region, which here is the superlattice. The miniband width is normally much smaller, than that of typical contacting leads. Therefore, in the actual energy interval, the variation of the lead-related Green functions can be regarded as negligible in most cases of interest. Thus, the only energy dependent quantities remaining in the transmission probability are those referred to the superlattice, i.e., to the Hamiltonian (1).

Combined together, the model assumptions yield³⁴

$$T(E, \mathcal{E}) = \frac{4A^2 G_{1,\mathcal{N}}^2(E)}{[1 + A^2 G_{\Delta}(E)]^2 + A^2 [G_{1,1}(E) - G_{\mathcal{N},\mathcal{N}}(E)]^2 + 4A^2 G_{1,\mathcal{N}}^2(E)}, \quad (2)$$

where $G_{\Delta}(E) = G_{1,1}(E)G_{\mathcal{N},\mathcal{N}}(E) - G_{1,\mathcal{N}}^2(E)$; and the (superlattice) Green function obeys the equation

$$\sum_{n''=1}^{\mathcal{N}} (E\delta_{n,n''} - H_{nn''}) G_{n''n''}(E) = \delta_{n,n'}. \quad (3)$$

In Eq. (2), the quantity $A \sim \mathcal{V}^2$ (independent of energy) associates with the weighted local density of states on the drain/source-superlattice interfacial surfaces. The Green function matrix elements, which appear in the above equations, depend on E_{\parallel} and \mathcal{E} . These are the only energy dependent quantities in Eq. (2) and therefore, here and henceforth the subscript in E_{\parallel} , as well as an indication of the Green function dependence on \mathcal{E} , are omitted for brevity. Analytical expressions of $G_{11}(E) = -G_{\mathcal{N}\mathcal{N}}(-E)$, and $G_{1\mathcal{N}}(E)$ are given by²³

$$D_{\mathcal{N}}(E, \mathcal{E})G_{11}(E) = J_{\mu+(\mathcal{N}-1)/2}(z)Y_{\mu-(\mathcal{N}+1)/2}(z) - Y_{\mu+(\mathcal{N}-1)/2}(z)J_{\mu-(\mathcal{N}+1)/2}(z), \quad (4)$$

$$D_{\mathcal{N}}(E, \mathcal{E}) = J_{\mu+(\mathcal{N}+1)/2}(z)Y_{\mu-(\mathcal{N}+1)/2}(z) - Y_{\mu+(\mathcal{N}+1)/2}(z)J_{\mu-(\mathcal{N}+1)/2}(z), \quad (5)$$

and $D_{\mathcal{N}}(E, \mathcal{E})G_{1\mathcal{N}}(E) = \mathcal{E}/\pi$, where $\mu \equiv E/\mathcal{E}$, $z \equiv 2/\mathcal{E}$, and $J_{\mu}(z)$ and $Y_{\mu}(z)$ are the Bessel functions of the first and second kind, respectively.

Before going into a detailed discussion of $T(E, \mathcal{E})$ dependence on energy, field strength, and superlattice length (the latter is not indicated explicitly), some relevant remarks might be useful. As is mentioned above, the n - E (length-energy) areas, which are classically accessible for electrons (shaded in Figs. 1 and 2) are distinct, depending on whether the electrostatic energy is smaller or larger, than the zero-field band width. For this reason, the voltages

restricted by the conditions $eV < E_{\text{bw}}$ and $eV > E_{\text{bw}}$ will be referred as *low* and *high* voltages, respectively. The qualitative difference between the two cases stems from that the electron states extended over the entire superlattice (indicated in the figures by 'es') can exist at low voltages, but not at high voltages, when the es-band is shrunken and the WS-band opens instead.

Contrary to extended states, which "connect" the source and drain electrodes, the electron states located within either of two triangular areas, are separated from the other side of the superlattice by a triangular barrier, see Fig. 2. (The field induced surface localized states exist if $\mathcal{E} \geq 12.2/\mathcal{N}^3$.²⁵) Two triangular barriers separate the states located within the WS-band. Hence, depending on the applied voltage and energy of electrons to be transmitted through the superlattice, the electron flux can encounter no barriers at all, one triangular barrier, two triangular barriers, or a trapezoid barrier, as is exemplified by arrows labeled in Fig. 2 by RT, FN, TB, and WS. The through trapezoid barrier (TB) tunneling, which also includes the Fowler-Nordheim (FN) regime of tunneling, has been extensively studied in the WKB approximation.³⁵ Such an approach is inapplicable for the description of the present discrete, finite band model. In particular, it fails to reproduce the resonance structure of $T(E, \mathcal{E})$, which might be expected for the sls-assisted tunneling (i.e., tunneling through a triangular well). For the resonance tunneling (RT) transmission, the energy and length dependence of $T(E, \mathcal{E})$ in zero field $\mathcal{E} = 0$ has been analyzed previously.³² However, the presence of electric field gives rise to new regularities which have not been studied so far. In what follows, the transmission spectrum will be examined in the RT, FN, WS, and TB energy intervals, where surprisingly accurate explicit expressions of $T(E, \mathcal{E})$ can be derived from the model exact equations (2), (4), and (5).

III. EXTENDED STATES ASSISTED TUNNELING

At low voltages the mid band levels can form WSLs with noncanonical level spacing²⁵

$$E_l = \left\{ \frac{l}{l + 1/2} \right\} \frac{1}{1 - 2m'/m} \mathcal{E}_{m'/m}, \quad (6)$$

where the upper (lower) factor should be used for an odd $\mathcal{N} = 2N + 1$ (even $\mathcal{N} = 2N$) number of wells in the superlattice; $l = 0, 1, 2, \dots; m$ and $m' < m/2$ are positive integers, which specify the value of the field parameter

$$(\mathcal{N} - 1) \mathcal{E}_{m'/m} = 4 \cos \left(\pi \frac{m'}{m} \right). \quad (7)$$

For some voltages, the correspondence between the approximate WSL energies and exact eigenvalues (solutions to $\mathcal{D}_{\mathcal{N}}(E, \mathcal{E}) = 0$) can be seen in Fig. 3, where the former and the latter are indicated by circles and stars, respectively. In our example, $\mathcal{N} = 101$; the increase/decrease of \mathcal{N} improves/worsens the accuracy of Eq. (6).

As is implied by the derivation of Eqs. (6) and (7),²⁵ the WSL with the level spacing, equal to \mathcal{E} times any but > 1 integer or ratio of two integers, appears in the spectrum mid under a voltage, determined by Eq. (7), within the range $0 < eV < E_{\text{bw}}$. This result may be thought as a reminiscence of approximately equidistant levels with the spacing equal to π/N near the center of zero-field band. For an experimental observation, the WSLs of the type $E_l = lq\mathcal{E}$, where q is equal to either a positive integer ≥ 2 or $1 + 2m'/(m - 2m')$ with a not too small second summand, are perhaps most meaningful, because the level spacing is well distinguishable from that in the canonical WSL. It also may be of importance from the experimental point of view that any of (noncanonical) WSLs can be obtained only at a unique voltage. For instance, the WSL with triple- \mathcal{E} level spacing should appear, when the electrostatic energy is exactly equal to $E_{\text{bw}}/2$, if \mathcal{N} is odd, or to $E_{\text{bw}}/2 - \mathcal{E}$, if \mathcal{N} is even. As we believe, these results can help to identify the electric field effects.

To obtain an explicit expression of $T(E, \mathcal{E})$, we use in Eq. (2) an approximation of the Green function matrix elements at the energies $E_n = n\mathcal{E}$ with n equal to a positive integer restricted by the condition $n \ll \mathcal{N}$. Performing some algebra, which is much in the spirit of the derivation of noncanonical WSLs,²⁵ we get instead of Eqs. (4) and (5)

$$G_{11}(E_n, \mathcal{E}) \approx \frac{\sin[(2n - 1)\chi]}{\sin(2n\chi)}, \quad (8a)$$

$$G_{\mathcal{N}\mathcal{N}}(E_n, \mathcal{E}) \approx -\frac{\sin[(2n + 1)\chi]}{\sin(2n\chi)}, \quad (8b)$$

$$G_{1N}(E_n, \mathcal{E}) \approx (-1)^{N+n+1} \frac{\sin \chi}{\sin(2n\chi)}, \quad (8c)$$

where $\chi = \arccos(\mathcal{E}N/2)$. Unlike the exact expressions for the Green function matrix elements, Eqs. (8a), (8b), and (8c) make sense only for large values of N (set to be odd), and only for the indicated energies. Using the above expressions in Eq. (2) we obtain

$$T(E = n\mathcal{E}, \mathcal{E}) \approx \frac{4A^2 \sin^2 \chi}{4A^2 \sin^2 \chi + \sin^2(2n\chi) [1 + 2 \cos(2\chi) A^2 + A^4]}, \quad (9a)$$

or, equivalently,

$$T(n\mathcal{E}, \mathcal{E}) \approx \frac{A^2(4 - \mathcal{E}^2 N^2)}{A^2(4 - \mathcal{E}^2 N^2) + \sin^2[2n \arccos(\mathcal{E}N/2)][(1 - A^2)^2 + A^2 \mathcal{E}^2 N^2]}. \quad (9b)$$

Note that Eq. (9a) is also valid for high voltages, in which case $\chi = \cosh^{-1}(\mathcal{E}N/2)$, and $\sin \chi$ and $\cos \chi$ should be replaced by $\sinh \chi$ and $\cosh \chi$, respectively.

According to Eq. (9b), if the applied potential satisfies Eq. (7), the transmission coefficient is equal to unit for $E = n\mathcal{E}$ with n divisible by m , if m is odd, or by $m/2$, if it is even. This result makes it obvious that $T(E, \mathcal{E})$ has a resonance-like structure, as a function of the applied voltage at a fixed energy and, as a function of energy at a fixed voltage. Thereby, noncanonical WSLs are exposed in the transmission spectrum, see Fig. 3, as almost equidistant peaks. It is seen that the level spacing is in a good agreement with formula (6) (the WSL energies are indicated in Fig. 3 by circles on the E-axis). However, the above approximation does not reproduce the decrease of transmission peak maxima, which is a pronounced tendency of the exact dependence of the transmission probability on energy. Represented by a few graphs in Fig. 3, it reflects a general trend of resonance tunneling phenomena, which implies the unit transmission probability only for totally symmetric systems (e.g., as conventional barrier-well-barrier symmetric heterostructures). In the given case, the system symmetry is broken by the applied potential, the increase of which results in an increasing suppression of the transmission peaks close to the es-band edges.

With the increase of superlattice-to-lead coupling parameter $|A|$, transmission peaks broaden, see Fig. 3, which is a kind of expected behavior from other resonance tunneling structures. Figure 3 also exposes intuitively not expected behavior of the transmission spectrum response to increasing voltage. As is clearly seen from the comparison of the peak positions for ever larger potential (from bottom to top), the peak spacing *decreases* with the *increase* of \mathcal{E} . So, in addition to a distinctive level spacing, and hence, peak spacing, which is characteristic for noncanonical WSLs, they are also distinguishable, from the experimental point of view, due to a specific field dependence of the transmission peak spacing. The latter decreases with eV , while in a canonical WSL it should increase.

IV. SURFACE LOCALIZED STATES ASSISTED TUNNELING

By using the standard approximations of Bessel functions with large arguments and small or large orders,³⁶ it can be shown that the exact expressions of $G_{11}(E)$, $G_{NN}(E)$, and $G_{1N}(E)$ [see Eqs. (4) and (5)] are accurately reproduced within the sls-band energy interval $|2 - eV/2| + \mathcal{E} < E < 2 + eV/2 - \mathcal{E}$ by the following relations

$$\left\{ \begin{array}{l} \mathcal{D}_N(E, \mathcal{E}) \\ \mathcal{D}_N(E, \mathcal{E})G_{11}(E, \mathcal{E}) \\ \mathcal{D}_N(E, \mathcal{E})G_{NN}(E, \mathcal{E}) \end{array} \right\} \approx \frac{\mathcal{E}/\pi}{\sqrt{\sin \xi \sinh \delta}} \exp\left(\frac{2}{\mathcal{E}} \Phi_\delta\right) \left\{ \begin{array}{l} \cos\left(\frac{2}{\mathcal{E}} \Phi_\xi - \frac{\pi}{4} + \xi\right) e^\delta \\ \cos\left(\frac{2}{\mathcal{E}} \Phi_\xi - \frac{\pi}{4} + \xi\right) \\ \cos\left(\frac{2}{\mathcal{E}} \Phi_\xi - \frac{\pi}{4}\right) e^\delta \end{array} \right\}, \quad (10)$$

where $2 \cosh \delta = E + eV/2$, $\Phi_\delta = \delta \cosh \delta - \sinh \delta$, $2 \cos \xi = E - eV/2$ ($0 \leq \xi \leq \pi$), and $\Phi_\xi = \sin \xi - \xi \cos \xi$. Note that the excluded \mathcal{E} intervals can contain not more, than one sls level each.

Using the above expressions for the Green function matrix elements in Eq. (2), we get

$$T(E, \mathcal{E}) = \frac{4A^2 \sinh \delta \sin \xi \exp(-2\delta)}{(1 + A^2 e^{-2\delta}) \left[\cos^2\left(\frac{2}{\mathcal{E}} \Phi_\xi - \frac{\pi}{4} + \xi\right) + A^2 \cos^2\left(\frac{2}{\mathcal{E}} \Phi_\xi - \frac{\pi}{4}\right) \right]} \exp\left(-\frac{4}{\mathcal{E}} \Phi_\delta\right), \quad (11)$$

showing a resonance-like structure modulated by a function $\exp(-4\Phi_\delta/\mathcal{E})$ that decays exponentially with the increase of energy.

For the energies of sls-band levels E_n^{sls} , given by solutions to equation $\mathcal{D}_N(E, \mathcal{E}) \sim \cos(2\Phi_\xi/\mathcal{E} - \pi/4 + \xi) = 0$ within the energy interval $|2 - eV/2|, 2 + eV/2|^{25}$ expression (11) simplifies to

$$T(E_n^{\text{sls}}, \mathcal{E}) = \frac{4 \sinh \delta_n \exp(-2\delta_n)}{\sin \xi_n [1 + A^2 \exp(-2\delta_n)]} \exp\left(-\frac{4}{\mathcal{E}} \Phi_{\delta_n}\right), \quad (12)$$

where $\delta_n = \cosh^{-1}(E_n^{\text{sls}}/2 + eV/4)$ and $\xi_n = \arccos(E_n^{\text{sls}}/2 - eV/4)$. In the case of weak superlattice-to-lead coupling $A^2 \ll 1$, Eq. (12) determines local maxima of $T(E, \mathcal{E})$. Thus with the replacement $E_n^{\text{sls}} \rightarrow E$, the r.h.s. of Eq. (12) gives a function enveloping peaks of the transmission spectrum in the region of sls-assisted tunneling.

As is seen in Fig. 4, except a small \mathcal{E} interval above the top of es- or WS-band, an explicit analytical description of the sls-assisted tunneling given by Eq. (11) is indistinguishable from exact calculations. This is a central result of the section. It might be worth emphasizing that details of the resonance structure of $T(E, \mathcal{E})$, such as the position of peaks, and their width and intensity, are model dependent. In contrast, factor $\exp(-4\Phi_\delta/\mathcal{E})$, which prescribes for the sls-assisted tunneling probability an exponential *decrease* with the increase of energy (counted from the spectrum center) and an exponential *increase* with the increase of electric field strength, is characteristic for the linear drop of the electrostatic potential within the scattering region and does not depend on a particular model of the interface (connection) with the leads. The reason for this is that sls-assisted tunneling is controlled by exponential tailing of the sls wave function in the classically forbidden region. Therefore, the exponential decay of the through sls-band tunneling probability can be evaluated from the ratio of the probabilities to find an electron with, say, the energy E_n^{sls} in the first and last wells of the isolated superlattice. Such an approach, which is much more simple technically (since the leads and connection to them are out of consideration), gives a reasonable result even for the pre-exponential factor of the enveloping function³⁷ $T(E_n^{\text{sls}}, \mathcal{E}) = (\sinh \delta_n / \sin \xi_n) \exp(-2\delta_n) \exp(-4\Phi_{\delta_n}/\mathcal{E})$, which differs from the correct expression (12) only by factor of four.

To make Eq. (11) easy readable, one can use an approximate expression

$$3\Phi_\delta \approx \begin{cases} (E - \overline{eV}/2)^{3/2}, & eV \leq E_{\text{bw}}, \\ (E + \overline{eV}/2)^{3/2}, & eV > E_{\text{bw}}, \end{cases} \quad (13)$$

where $\overline{eV} = |eV - E_{\text{bw}}| = |eV - 4|$ is the excess of electrostatic potential energy over zero-field band width, and $\overline{eV}/2$ has the meaning of the top of es-band (WS-band) for low (high) voltages. The above approximation reproduces the exact dependence reasonably well up to \overline{eV} of the order of E_{bw} , see Fig. 5.

Using Eq. (13) in Eq. (11), the exponential factor $\exp(-4\Phi_\delta/\mathcal{E})$ can be replaced, if $eV < E_{\text{bw}}$, by $\exp[-4(E - \overline{eV}/2)^{3/2}/(3\mathcal{E})]$, which is identical to that appears in the Fowler-Nordheim theory of field emission.³⁸ At high voltages, however, factor $\exp[-4(E + \overline{eV})^{3/2}/(3\mathcal{E})]$ does not have a semi-classical analogy. In some more details, links of Eq. (11) with the probability of tunneling through a triangular barrier are discussed in Ref. 37.

A. Effects of coupling on sls transmission spectrum

The superlattice-to-lead connection (represented in Eq. (11) by a single parameter A) is dependent on a number of factors. For this reason, in relevant heterostructures the magnitude of effective coupling $|A|$ may vary by orders. It is of interest therefore, to trace the dependence of the sls-band transmission spectrum on the coupling strength.

A common expectation is that with the increase of coupling strength the resonance structure is smeared out. This is really true for resonance tunneling in zero field. By contrast, as can be readily seen from Eq. (11), such an expectation is not justified for sls-assisted tunneling. In the latter case, the peak position and their sharpness is essentially determined by two cosine terms in the denominator of r.h.s. in Eq. (11). In the absence of anyone of the two, the transmission spectrum would contain infinitely high resonances either at the sls energies E_n^{sls} ($A = 0$, the extreme case of weak coupling) or at zeros of $\cos(2\Phi_\xi/\mathcal{E} - \pi/4)$ (the extreme case of strong coupling).

If the coupling is weak, the peak spacing repeats the level spacing within sls-band. In due course, the latter is proportional to \mathcal{E} , $2\mathcal{E}$, and ruled by poles of the Airy function, within the lower, mid, and upper part of the sls-band, respectively.²⁵ These regularities can thus be observed in the sls-band transmission spectrum, as is illustrated in Fig. 4a by open circles (\mathcal{E} spacing), filled circles ($2\mathcal{E}$ spacing), and squares (Airy type spectrum).

In the case of strong coupling $A^2 \gg 1$, the position of peaks in $T(E, \mathcal{E})$ is determined by zeros of the second summand of the denominator in Eq. (11), and we have instead of Eq. (12)

$$T(E_p, \mathcal{E}) = \frac{4 \sinh \delta_p}{\sin \xi_p} \exp \left(-\frac{4}{\mathcal{E}} \Phi_{\delta_p} \right), \quad (14)$$

where the values of E_p are given by solutions to equation $\cos(2\Phi_\xi/\mathcal{E} - \pi/4) = 0$. These are shifted with respect to sls energies E_n^{sls} , and can be shown to obey the same regularities as those, observed for the eigenvalues. The height of peaks does not differ much in the cases of strong and weak coupling, as can be seen from comparison of Eqs. (12) and (14). At the same time, if $|A|$ is large, the wells between peaks are approximately A^2 times deeper. Summarizing, in the case of sls-assisted tunneling, strong coupling with the leads makes the resonance structure of the transmission spectrum even more pronounced. Otherwise, the weak and strong coupling result in a similar structure of the transmission spectrum with identical regularities of the peak spacing dependence on the electric field, see Fig. 6.

On the other hand, it follows from Eq. (11) that the resonance structure will be essentially smeared out in the case of intermediate coupling strength, when $|A| \approx 1$. This unusual behavior of sls-band transmission spectrum is illustrated by calculations of $T(E, \mathcal{E})$ for different couplings, $|A| \ll 1$, $|A| = 1$, and $|A| \gg 1$ in Fig. 4b. One can see that with the increase of coupling strength, the transmission spectrum, at first, loses its resonance structure, and then acquires it again with, roughly, interplaced peaks and wells, and deepened wells.

The above analysis shows that the resonance tunneling assisted by surface localized states, which appear as a result of the band tilting by the applied voltage, is characterized by a kind of unique (at least, met not often) dependence of the transmission spectrum on the coupling with electron reservoirs from and to which the tunneling occurs.

Some minimal voltage is required for the first sls to appear and hence, sls-assisted tunneling to be possible. Further increase of the applied potential results in sls-band opening up to its maximal width E_{bw} . The increase of sls-band width is accompanied by the appearance of peaks in $T(E, \mathcal{E})$ with the spacing governed by the following regularities. For $eV < E_{\text{bw}}/2$, the peak spacing is close to that of Airy spectrum. For $E_{\text{bw}}/2 < eV < E_{\text{bw}}$, the Airy type peak spacing gradually changes to the double \mathcal{E} peak spacing characteristic for $H_{nn'}$ eigenvalues in the mid of the maximal-width sls-band. Finally, for $eV > E_{\text{bw}}$, there exists the third characteristic energy interval (close to the top of WS-band), where peaks of the transmission probability are \mathcal{E} -spaced. The latter spacing is commonly regarded as the WSL trademark.

V. WANNIER-STARK STATES ASSISTED TUNNELING

In the energy interval of bulk states (i.e., in the mid of the full spectrum), switching from the low to high voltages results even in a more profound restructuring of the transmission spectrum. This can be expected since the es-band, which directly connects the source and drain leads, is replaced by the WS-band, where the electronic states are localized between two mutually inverse triangular barriers. Tunneling through es-band was already discussed in Sec. 3. Treatment of WS-states assisted tunneling, which refers to the energy interval $E < eV/2 - \mathcal{E}$, is similar to the preceding analysis.

In the present case, however, large \mathcal{N} , explicit expressions of the Green function matrix elements are different for the eigenvalue energies E_n (up to exponentially small corrections given by $E_n \approx n\mathcal{E}^{25}$) and for $E \neq E_n$. For the latter (and $\mathcal{N} = 2N + 1$), we have

$$\left\{ \begin{array}{l} \mathcal{D}_{\mathcal{N}}(E, \mathcal{E}) \\ \mathcal{D}_{\mathcal{N}}(E, \mathcal{E})G_{11}(E, \mathcal{E}) \\ \mathcal{D}_{\mathcal{N}}(E, \mathcal{E})G_{NN}(E, \mathcal{E}) \end{array} \right\} \approx \frac{(-1)^N \mathcal{E} \sin(\pi E/\mathcal{E})}{\pi \sqrt{\sinh \delta \sinh \delta'}} \exp \left(\frac{2}{\mathcal{E}} \Phi^+ \right) \left\{ \begin{array}{l} e^{\delta+\delta'} \\ e^{\delta'} \\ -e^{\delta} \end{array} \right\}, \quad (15)$$

where $2 \cosh \delta' = eV/2 - E$, $\Phi^+ = \Phi_\delta + \Phi_{\delta'}$, and $\Phi_{\delta'} = \delta' \cosh \delta' - \sinh \delta'$. The use of Eq. (15) in Eq. (2) yields an explicit expression

$$T(E, \mathcal{E}) \approx \frac{4A^2 \sinh \delta \sinh \delta'}{\sin^2(\pi E/\mathcal{E}) \left\{ [\exp(\delta + \delta') - A^2]^2 + A^2 (\exp \delta + \exp \delta')^2 \right\}} \exp \left(-\frac{4}{\mathcal{E}} \Phi^+ \right), \quad (16)$$

which provides an accurate description of the tunneling probability within WS-band except the above indicated \mathcal{E} interval and energies close to values of $n\mathcal{E}$, see Fig. 6. For the eigenenergies, we have instead of Eq. (16)

$$T(n\mathcal{E}, \mathcal{E}) \approx \frac{4 \sinh \delta_n \exp[-2(\delta_n - \delta'_n)]}{\sinh \delta'_n [1 + A^2 \exp(-2\delta_n)]} \exp \left(-\frac{4}{\mathcal{E}} \Phi_n^- \right), \quad (17)$$

where $\Phi_n^- = \Phi_{\delta_n} - \Phi_{\delta'_n}$, $2 \cosh \delta_n = eV/2 + n\mathcal{E}$, and $2 \cosh \delta'_n = eV/2 - n\mathcal{E}$.

In the case of weak coupling, Eq. (17) has the same meaning for the WS-band, as Eq. (12) for the sls-band; and under the replacement $n\mathcal{E} \rightarrow E$ (hence, $\delta_n, \delta'_n, \Phi_n^- \rightarrow \delta, \delta', \Phi^- = \Phi_\delta - \Phi_{\delta'}$, respectively) the function $T(E, \mathcal{E})$ defined in Eq. (17) envelopes the transmission spectrum over its local maxima. The envelope is reproduced equally well by Eq. (9a) with the replacement of the trigonometric functions, which appear in expression (9a), by their hyperbolic counterparts.

By analogy, the expression of the transmission coefficient, that follows from Eq. (16) at the energies $E_n = (n+1/2)\mathcal{E}$ (for odd \mathcal{N}), may be called minima envelope. Its expression is given by

$$T(E, \mathcal{E}) \approx \frac{4A^2 \sinh \delta \sinh \delta'}{[\exp(\delta + \delta') - A^2]^2 + A^2 (\exp \delta + \exp \delta')^2} \exp\left(-\frac{4}{\mathcal{E}} \Phi^+\right). \quad (18)$$

The maxima- and minima-enveloping functions shown in Fig. 6 exhibit a striking difference in their dependence on energy. The reason for this can be exposed by using approximation (13) and its analogue for $\Phi_{\delta'}$

$$3\Phi_{\delta'} \approx (\overline{eV}/2 - E)^{3/2}, \quad (19)$$

the accuracy of which is illustrated in Fig. 5. The exponents of the enveloping functions are thus defined simply as a difference $(4\Phi^-/\mathcal{E})$ and sum $(4\Phi^+/\mathcal{E})$ of two FN-type exponents $4(\overline{eV}/2 + E)^{3/2}/(3\mathcal{E})$ and $4(\overline{eV}/2 - E)^{3/2}/(3\mathcal{E})$. Notice, Eqs. (13) and (19) meet the requirements $\Phi^- = 0$, $\Phi^+ = 2\Phi_\delta^{\min} = \overline{eV}^{3/2}/(3\sqrt{2})$ at the mid of WS-band $E = 0$, and $\Phi^+ = \Phi^- = \Phi_\delta^{\max} = \overline{eV}^{3/2}/3$ at the top of WS-band $E = \overline{eV}/2$. These estimates makes it easily quantifiable a huge quantitative difference between maxima- and minima-envelope in the mid of WS-band.

An extremely sharp resonance structure, exhibited by the transmission spectrum of WS-states assisted tunneling, has the same nature as a well-known phenomenon of resonance tunneling through a barrier-well-barrier structure. In the given case, the barriers are of a triangular shape. The structure is totally symmetric (and the transmission coefficient is equal or close to unit for odd and even \mathcal{N} , respectively) only at the spectrum mid $E = 0$. The increase/decrease of energy strongly suppresses local maxima of electron transmission because of increasing system asymmetry. In contrast, because the total length of the two barriers is independent of energy, the minima envelope of $T(E, \mathcal{E})$ depends on energy not that strongly.

As can be concluded from Eqs. (17) and (18) and is exemplified in Fig. 6, unlike sls-assisted tunneling, the sharpness of resonance structure in the case of through WS-band electron transmission, to a large extent, is insensitive to the coupling strength. Hence, provided the symmetry conditions are met, tunneling through the mid part of a tilted band may serve as a nearly ideal energy filter. The anomalous sharpness and exponential decrease of the equidistant peaks also can be regarded as a distinctive signature of Bloch oscillations in through tilted band tunneling and related phenomena.

VI. THROUGH TRAPEZOID BARRIER TUNNELING

To wind up the discussion, we briefly consider the case of tunneling indicated in Fig. 2 by TB arrow. For energies outside the tilted band, $E > 2 + eV/2$, and for large \mathcal{N} , small \mathcal{E} , the transmission probability (2) can be shown to take the form

$$T(E, \mathcal{E}) = \frac{16A^2 \sinh \alpha \sinh \delta \exp[-2(\alpha + \delta)]}{1 + A^2[\exp(-2\alpha) + \exp(-2\delta)] + A^4 \exp[-2(\alpha + \delta)]} \exp\left[-\frac{4}{\mathcal{E}} (\Phi_\delta - \Phi_\alpha)\right], \quad (20)$$

where the definition of α differs from that of δ' only by interreplacement $E \leftrightarrow eV/2$, $2 \cosh \alpha = E - eV/2$. Under the indicated restrictions, the energy and field dependence, given by the above relation (solid lines in Fig. 7), is in excellent agreement with the model exact Eq. (2), except energies close to the sls-band, where Eq. (20) predicts the probability of tunneling which is somewhat different from exact values of $T(E, \mathcal{E})$ (not seen in the scale used).

Equation (20) and particularly, the exponential factor $\exp[-4(\Phi_\delta - \Phi_\alpha)/\mathcal{E}]$ looks very much differently from the usual WKB expression of probability to tunnel through a trapezoid barrier. Nevertheless, the WKB result can be retrieved from Eq. (20) by passing to the continuous limit, in the same way, as the FN exponential factor can be obtained from Eq. (11).³⁷ Skipping quite boring calculations, we present only the final result for the WKB equivalent of Eq. (20) (dashed line in Fig. 7)

$$T_{\text{WKB}}(E, eV) = \frac{16A^2 \sinh^2 \delta \exp(-2\delta)}{[1 + A^2 \exp(-2\delta)]^2} \exp\left[-2\delta\mathcal{N}\left(1 - \frac{eV}{4\delta^2}\right)\right]. \quad (21)$$

In zero field limit, Eq. (20) transforms into

$$T^{(0)}(E) = \frac{16A^2 \sinh^2 \delta^{(0)} \exp(-2\delta^{(0)})}{[1 + A^2 \exp(-2\delta^{(0)})]^2} \exp\left(-2\delta^{(0)}\mathcal{N}\right), \quad (22)$$

where $2 \cosh \delta^{(0)} = E$. Hence, without the second term in the exponent in Eq. (21), the WKB and zero-field expressions of $T(E, \mathcal{E})$ coincide in their functional dependence on δ and $\delta^{(0)}$, i.e., on the imaginary electron wave vector within the barrier. This proves the identity of $T_{\text{WKB}}(E, eV)$ with Eq. (20) in zero field limit. Moreover, as could be expected, the WKB expression fairly well describes tunneling through a trapezoid barrier, capped by an (energy bounded) tilted band, up to eV values comparable with E_{bw} , see Fig. 7, but not the case of high voltages.

So, Eqs. (20), (11), and (16) give an accurate explicit description of electron tunneling specified in Fig. 2 by TB, FN, and WS arrows, respectively. The latter equation corresponds to a purely quantum case and therefore, it does not have a semi-classical analogue, as do the two former equations. For the es-band, the resonance structure of the transmission spectrum is shown to contain, at certain voltages, evenly spaced peaks of noncanonical WSLs the existence of which has been predicted in Ref. 25.

VII. CONCLUSION

The transmission probability, describing electron ballistic transport between two leads connected electronically via a single tilted band, is presented as an explicit function of electron energy, electric field parameter, thickness of the contact (given by a superlattice, dielectric layer, or relevant) and parameter of lead effective coupling to the contacting region. The derived expressions bring to light all characteristic dependencies of the tunnel event, making every point, one would like to know about this particular model of electric field effects on tunneling, easy for the understanding. A number of conclusions is made throughout the discussion and their manifold physical and experimental implications are illustrated in various ways. No doubt that all of them were to an extent present in numerous related studies but had never been exposed with the present degree of explicitness and completeness covering all typical situations consistent with the model. The potential application of obtained results and methodology of their derivation is even more promising. Next challenge is to describe the Zener tunneling and Franz-Keldysh effect in finite, particularly, ultra-thin structures. Work in this direction is currently in progress.

ACKNOWLEDGMENTS

Support from the Swedish Research Council is greatfully acknowledged.

-
- ¹ G.H. Wannier, Phys. Rev. **117** (1960) 432.
² G.H. Wannier, Rev. Mod. Phys. **34** (1962) 645.
³ E.E. Mendez and G. Bastard, Physics Today **46** (6), 34 (1993).
⁴ F. Rossi, Semicond. Sci. Technol. **13** (1998) 147.
⁵ K. Leo, Semicond. Sci. Technol., **13** (1998) 249.
⁶ D.H. Dunlap and M.V. Kenkre, Phys. Rev. B **25** (1986) 3625.
⁷ M. Holthouse, Phys. Rev. Lett. **69** (1992) 351.
⁸ M. Holthouse, Z. Phys. B **89** (1992) 251.
⁹ M. Holthouse and D. Hone, Phys. Rev. B **69** (1993) 6499.
¹⁰ S.R. Wilkinson, C.F. Bharucha, K.W. Madison, Q. Niu, and M.G. Raizen, Phys. Rev. Lett. **76** (1996) 4512.
¹¹ Q. Niu, X.-G. Zhao, G.A. Georgakis, and M.G. Raizen, Phys. Rev. Lett. **76** (1996) 4504.
¹² M.G. Raizen, C. Salomon, and Q. Niu, Physics Today **50** (7), 30 (1997).
¹³ K.W. Madison, M.C. Fischer, R.B. Diener, Q. Niu, and M.G. Raizen, Phys. Rev. Lett. **81** (1998) 5093.
¹⁴ K.W. Madison, M.C. Fischer, and M.G. Raizen, Phys. Rev. A **60** (1999) R1767.
¹⁵ M. Glück, M. Hankel, A.R. Kolovsky, and H.J. Korsch, Phys. Rev. A **61** (2000) 061402(R).
¹⁶ J. Zak, Phys. Rev. Lett. **20** (1968) 1477.
¹⁷ K. Hacker and G. Obermair, Z. Physik **234** (1970) 1.
¹⁸ G.C. Stey and G. Gusman, J. Phys. C: Solid State Phys. **6** (1973) 650.
¹⁹ M. Saitoh, J. Phys. C: Solid State Phys. **6** (1973) 3255.

- ²⁰ H. Fukuyama, R.A. Bari, and H.C. Fogedby, Phys. Rev. B **8** (1973) 5579.
- ²¹ Yu.B. Gaididei and A.A. Vakhnenko, Phys. stat. sol. (b) **122** (1984) 239.
- ²² A.I. Onipko, L.I. Malysheva, and Yu.A. Klimenko, Physica B **225** (1996) 125.
- ²³ L.I. Malysheva, Ukr. Fiz. Zh. **45** (2000) 1475.
- ²⁴ V.M. Yakovenko and H.-S. Goan, Phys. Rev. B **58** (1998) 8002.
- ²⁵ A. Onipko and L. Malysheva, Solid State Commun. **118**, 63 (2001); Phys. Rev. B **63** (2001).
- ²⁶ D.L. Smith and S.M. Kogan, Phys. Rev. B **54**, 10354 (1996), and references therein.
- ²⁷ R. Landauer, IBM J. Res. Develop. **1**, 323 (1957); Philos. Mag. **21** (1970) 683.
- ²⁸ M. Büttiker, Y. Imry, R. Landauer, and S. Pinhas, Phys. Rev. B **31** (1985) 6207.
- ²⁹ A.D. Stone and A. Szafer, IBM J. Res. Develop. **32** (1988) 384.
- ³⁰ S. Datta, *Electronic Transport in Mesoscopic Systems* (Cambridge University Press, Cambridge, 1995).
- ³¹ C. Caroli, R. Combescot, P. Nozieres, and D. Saint-James, J. Phys. C: Solid State Phys. **4** (1971) 916.
- ³² V. Mujica, M. Kemp, and M. A. Ratner, J. Chem. Phys. **101**, 6849; **101** (1994) 6856.
- ³³ A. Onipko, Phys. Rev. B **59** (1999) 9995.
- ³⁴ A. Onipko, Yu. Klymenko, and L. Malysheva, Phys. Rev. B **62** (2000) 10480.
- ³⁵ J.G. Simmons, J. Appl. Phys. **34** (1963) 1793.
- ³⁶ M. Abramowitz and I.A. Stegun, *Handbook of Mathematical Functions* (New York: Dover, 1965).
- ³⁷ A. Onipko and L. Malysheva, Proceedings of Molecular Electronics 2000, Kona, Hawaii, December 10–14, 2000, to be published.
- ³⁸ R.H. Fowler and L. Nordheim, Roy. Soc. Proc. A **119** (1928) 173.

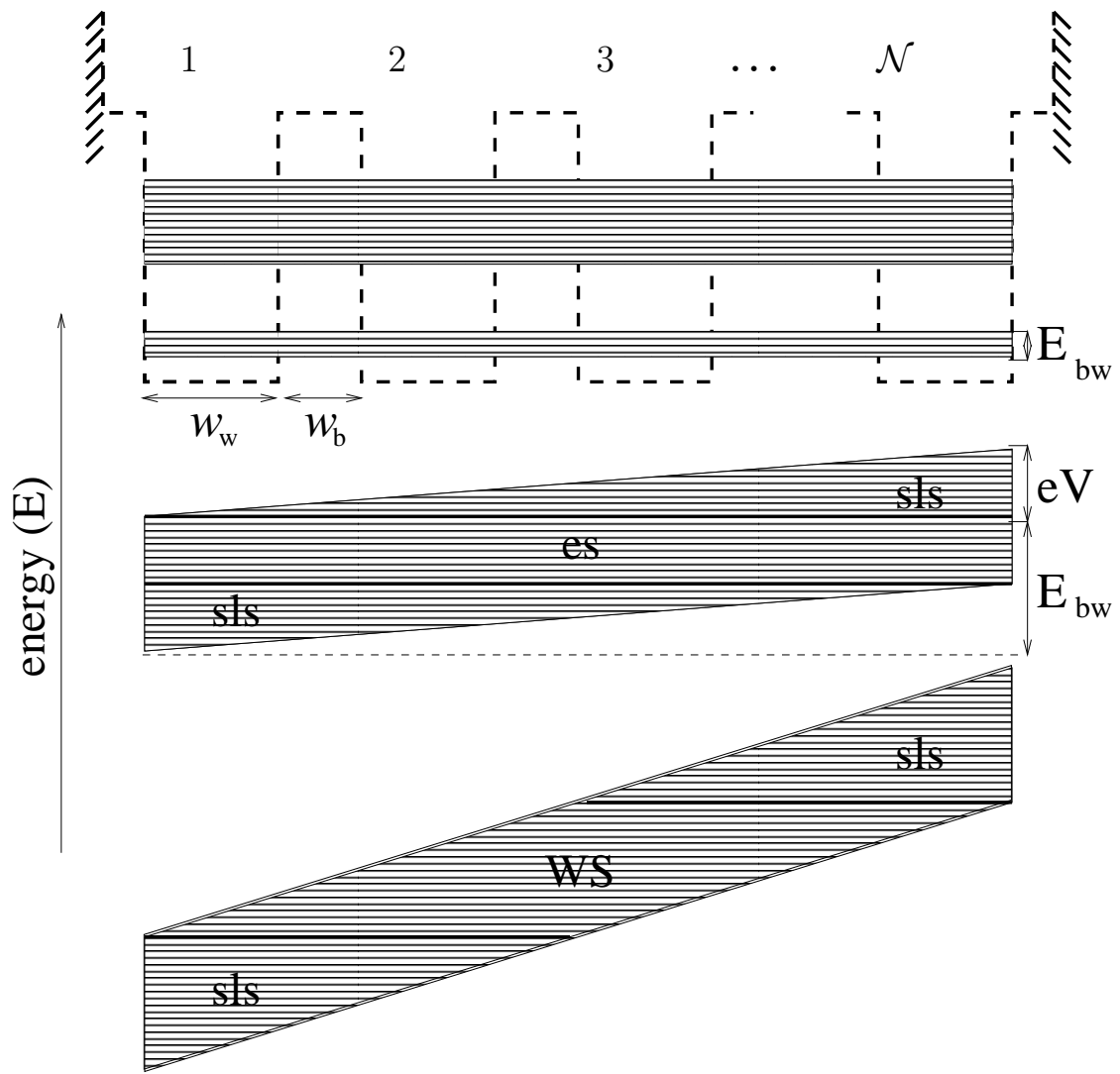


Fig. 1

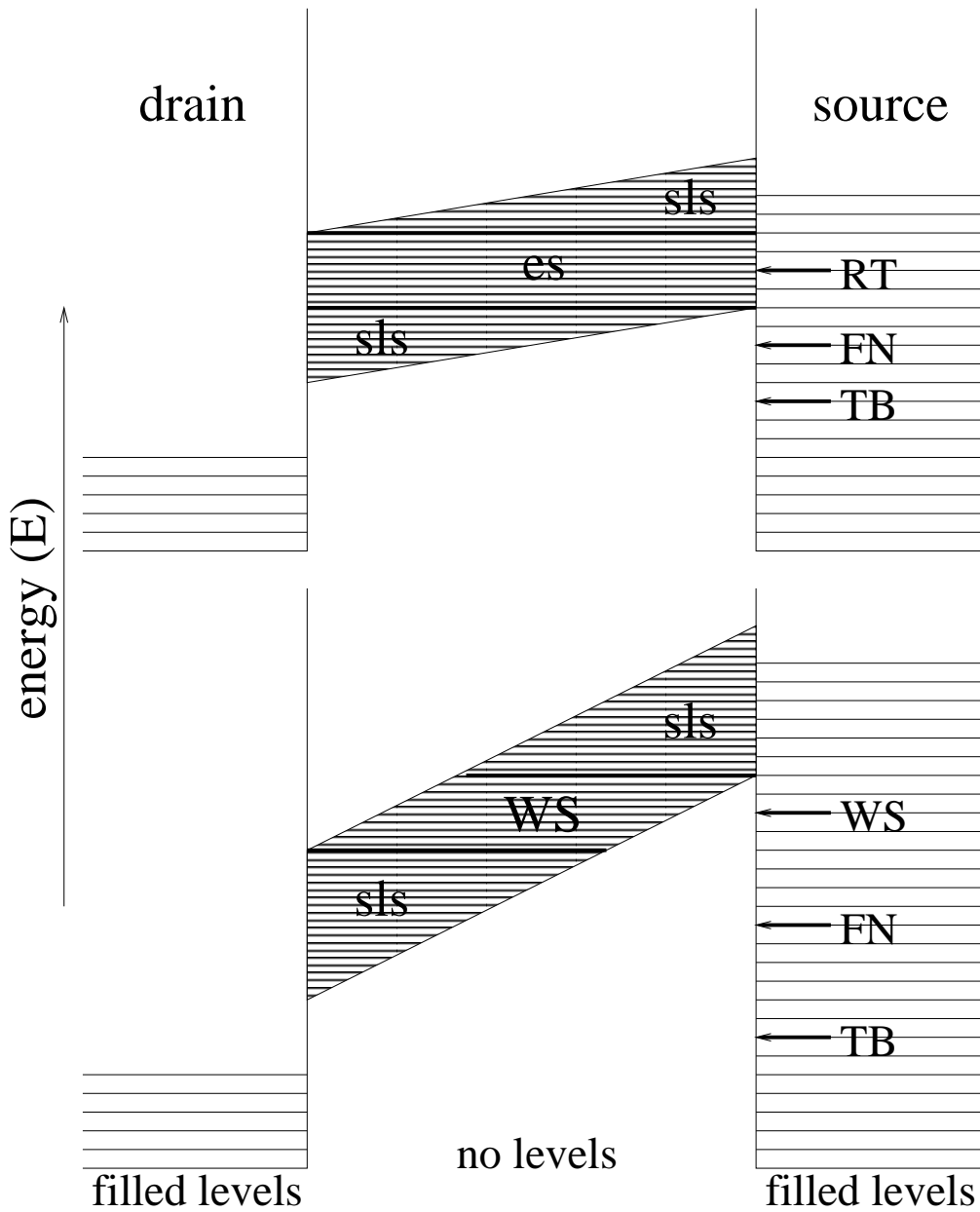


Fig. 2

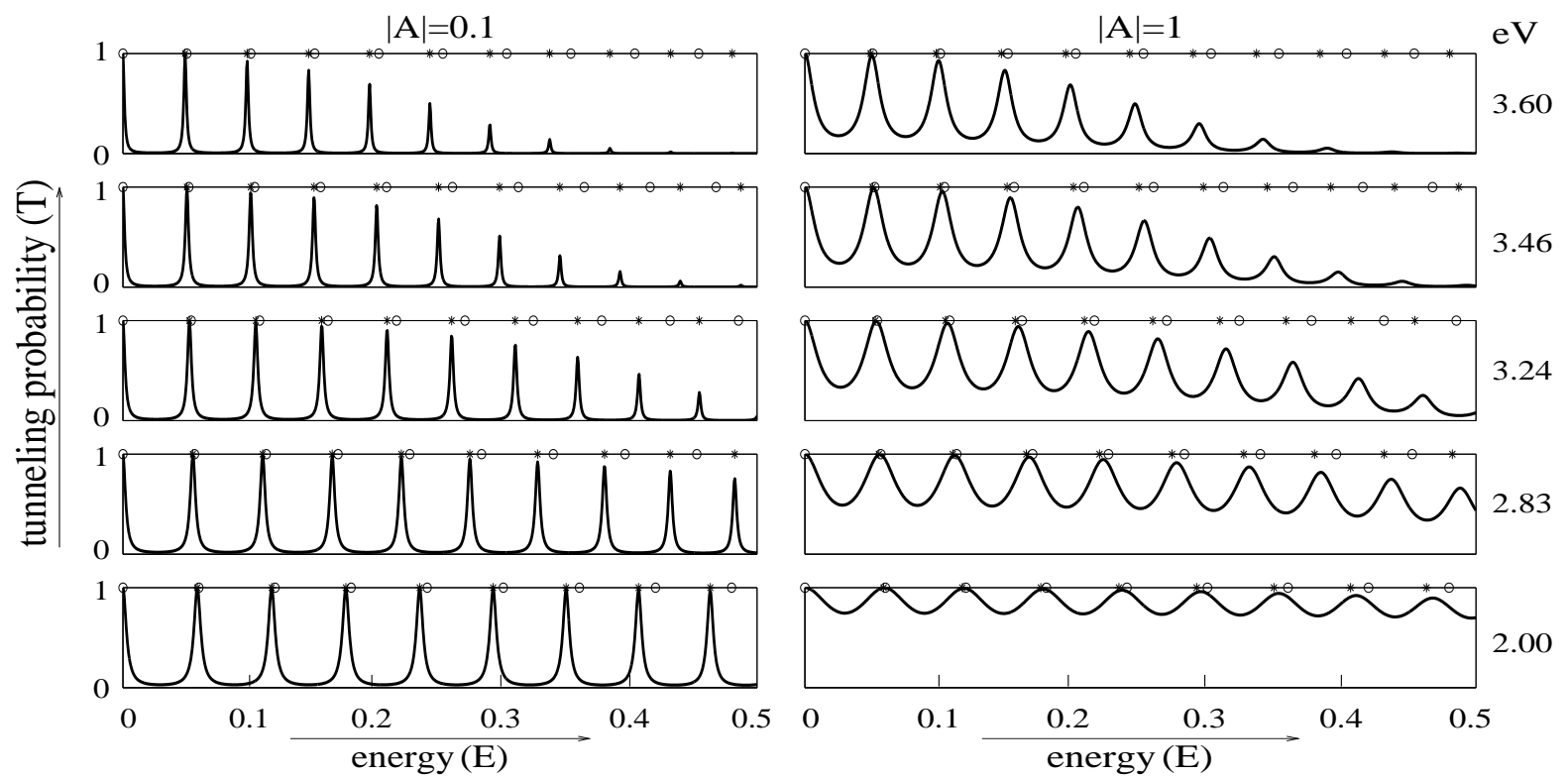
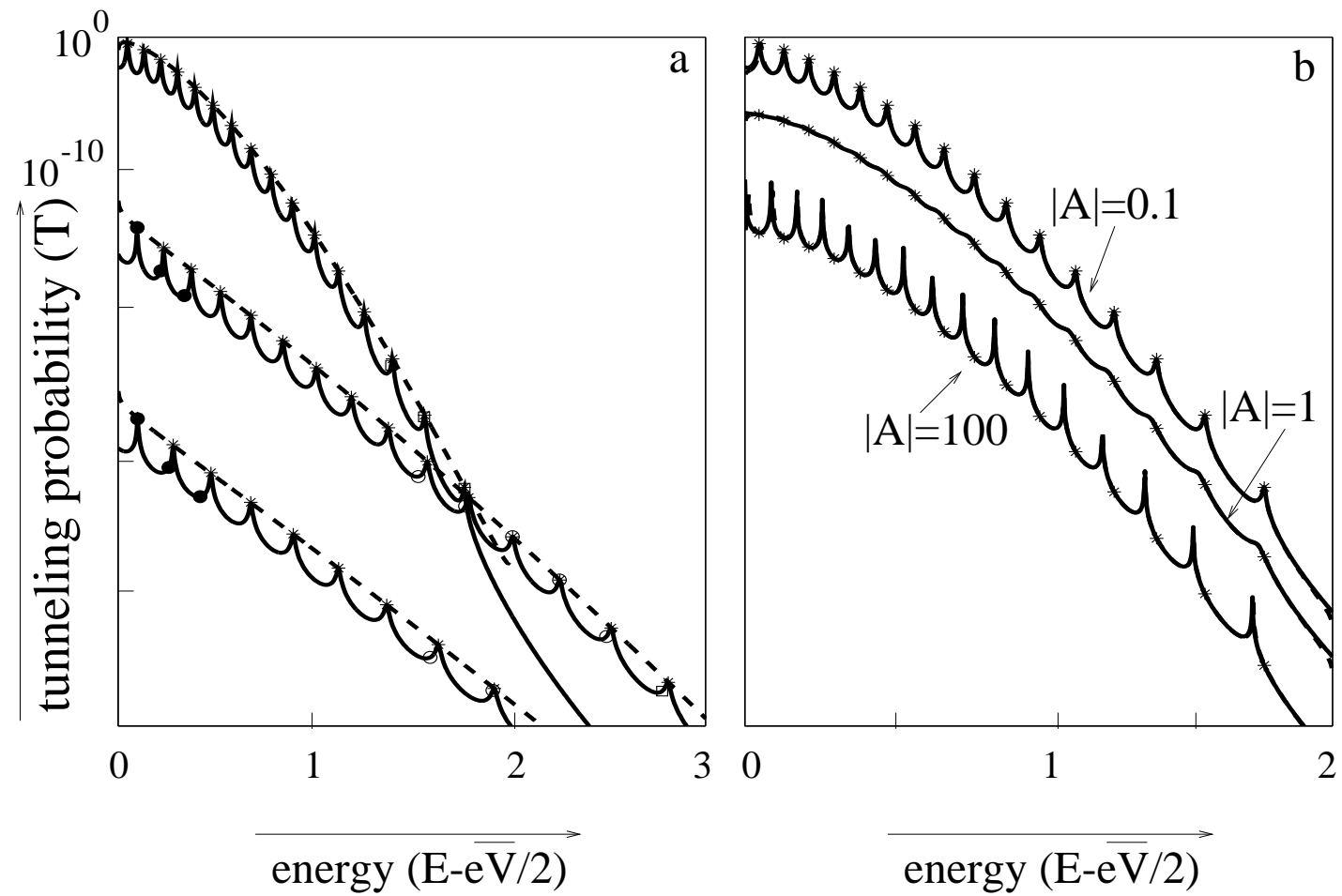


Fig. 4



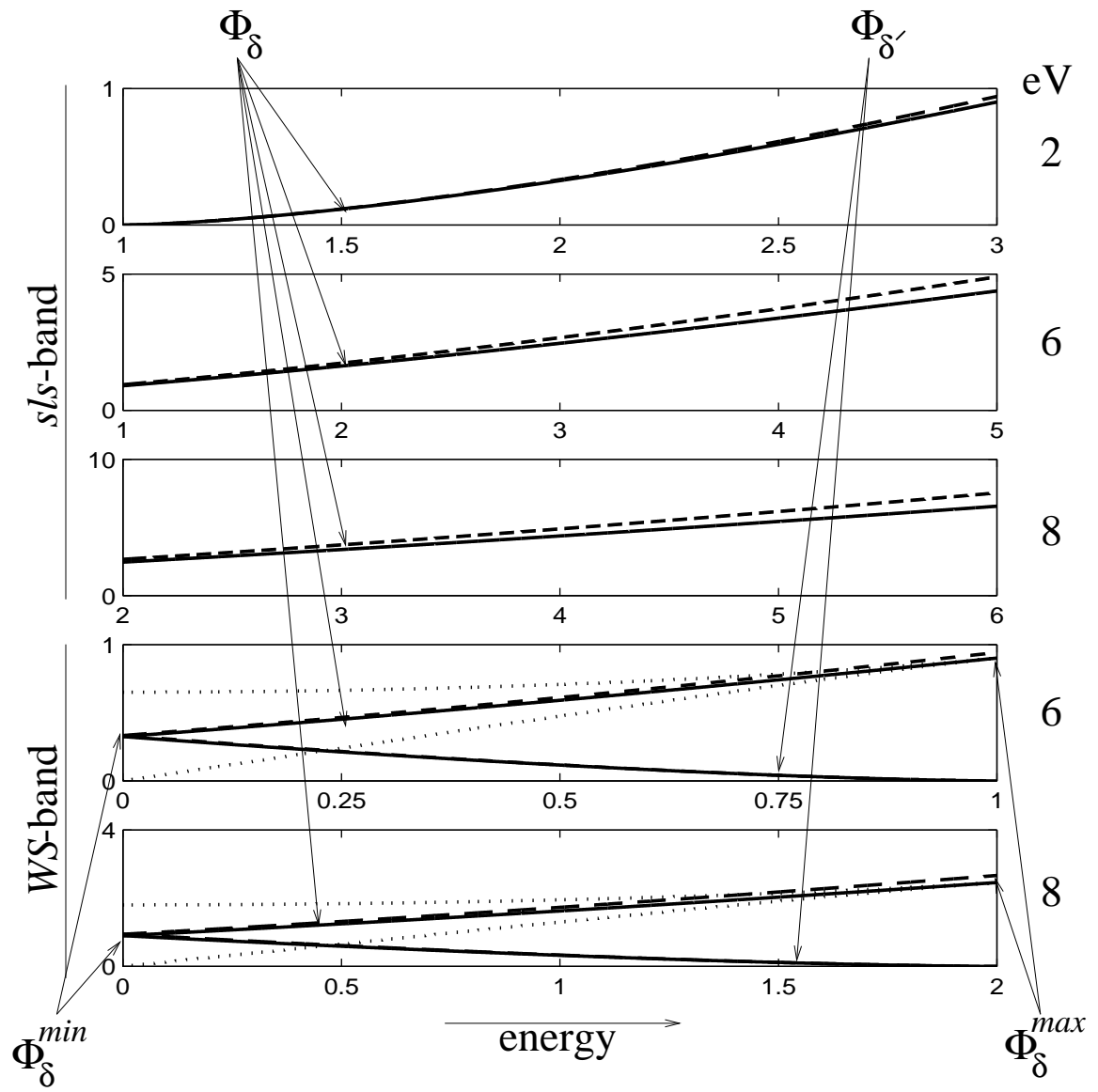
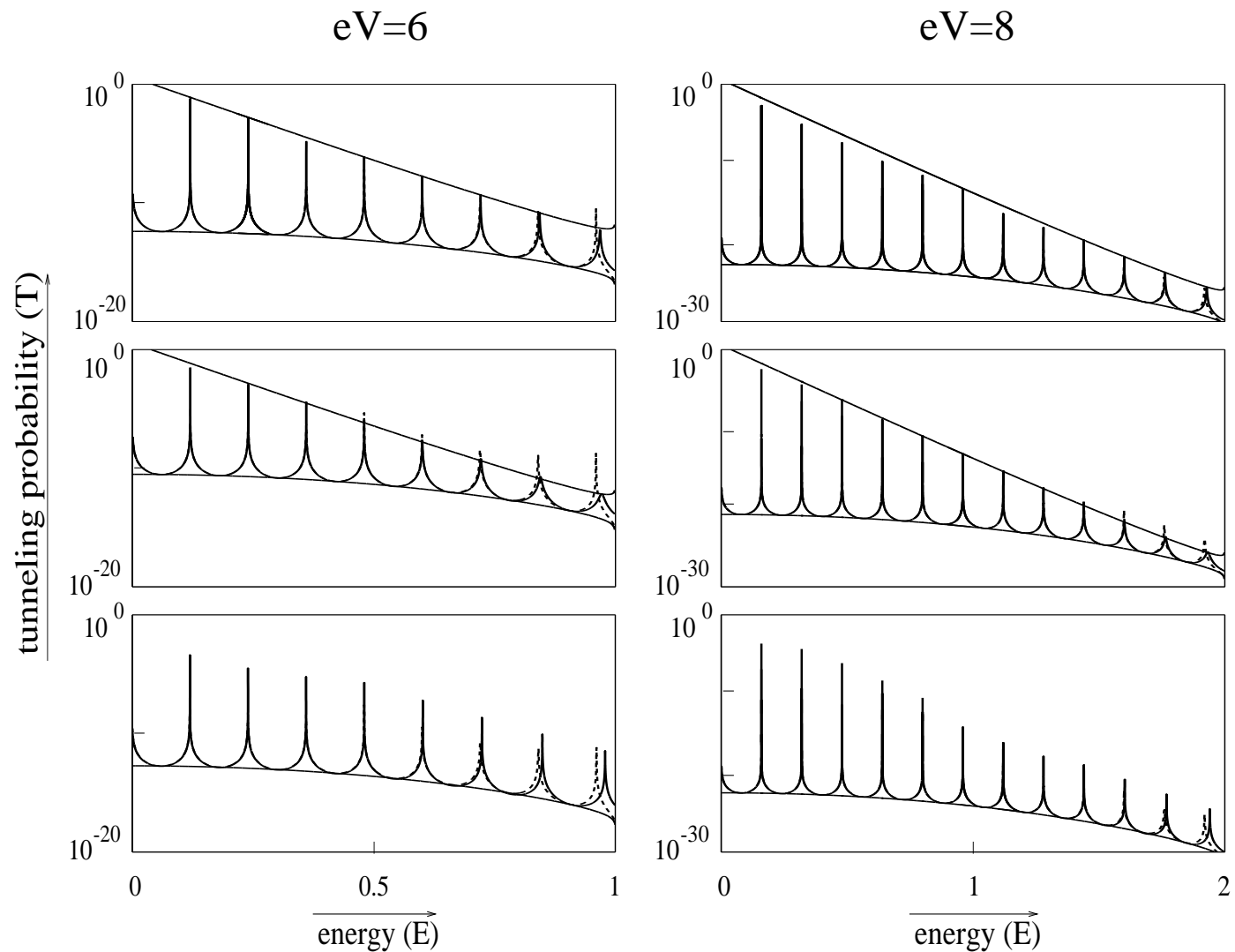


Fig. 5

Fig. 6



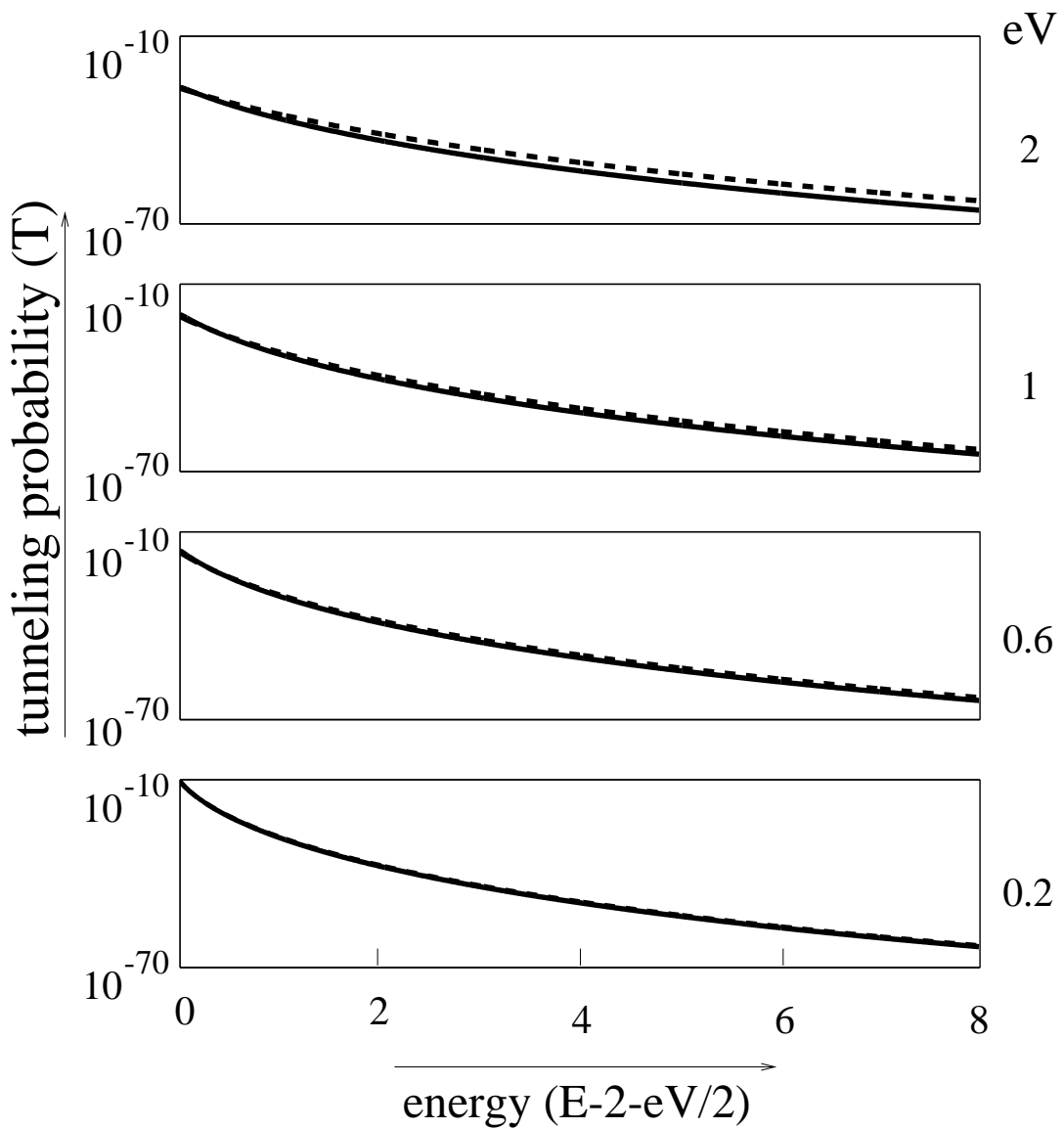


Fig. 7

Figure caption

Fig. 1. Upper part: potential energy profile of an \mathcal{N} -well superlattice and its two lowest minibands appearing due to the inter-well tunneling. For a superlattice $(\text{Al}_x\text{Ga}_{1-x}\text{AsAl}_{x^*}\text{Ga}_{1-x^*}\text{As})_{\mathcal{N}}$ with the well width $w_w = 100 \text{ \AA}$, barrier width $w_b = 40 \text{ \AA}$, barrier height = 0.3 eV, and electron effective mass = $0.066m_e$, the lowest miniband width (for $\mathcal{N} \gg 1$) $E_{bw} = 3.7 \text{ meV}$, which is 24 times smaller, than the band gap.⁸

Lower part: The lowest miniband tilted by the applied potential eV , which is smaller (up) and larger (down) than E_{bw} .

Fig. 2. Energy diagrams of lead-superlattice-lead heterostructure. Electronic spectrum of the superlattice is modeled by a single tilted band. At low voltages $eV < E_{bw}$ (upper diagram), the electron energy can be tuned to es-band (resonance tunneling, RT arrow), sls-band (Fowler-Nordheim type tunneling, FN arrow), or it can be out of the tilted band spectrum (through trapezoid barrier tunneling, TB arrow). The high voltage case is distinct only by that tunneling through the mid part of tilted band is assisted by Wannier-Stark states (WS arrow).

Fig. 3. Miniband transmission spectrum evolution under increasing voltage: from bottom to top $eV = 2.00, 2.83, 3.24, 3.46$, and 3.60 ; $\mathcal{N} = 101$. The exact level energies, i.e., solutions to $D_{\mathcal{N}}(E, \mathcal{N}) = 0$, are indicated by stars. WSLs with noncanonical level spacing $3\mathcal{E}_{1/3}$, $2\mathcal{E}_{1/4}$, $\frac{5}{3}\mathcal{E}_{1/5}$, $\frac{3}{2}\mathcal{E}_{1/6}$, and $\frac{7}{5}\mathcal{E}_{1/7}$ are labeled by open circles.

Fig. 4. Transmission spectrum of sls-assisted tunneling through the lowest miniband of a 51-well superlattice.
a) The miniband is tilted by the electrostatic potential difference eV of (up to down) $0.5E_{bw}$, $1.5E_{bw}$, and $2E_{bw}$; $|A| = 0.1$ (weak coupling). Open and filled circles indicate \mathcal{E} - and $2\mathcal{E}$ -spaced peaks; and those peaks, which follow the Airy spectrum $2 + eV/2 - E_n = [3\pi(n - 1/4)\mathcal{E}/2]^{2/3} - \mathcal{E}$,²⁵ are indicated by squares. Dashed envelopes represent Eq. (12) with E_n^{sls} replaced by E .
b) $T(E, \mathcal{E})$ is calculated from Eq. (2) (solid lines) and Eq. (11) (dashed line) for $eV = 0.5E_{bw}$ and $|A| = 0.1$ (weak coupling), 1 (intermediate coupling), and 100 (strong coupling). In both figures (a) and (b), stars indicate the values of $T(E_n^{\text{sls}}, \mathcal{E})$.

Fig. 5. Exact (solid lines) and approximate (dashed lines) dependencies $\Phi_{\delta}(E)$ and $\Phi_{\delta'}(E)$ as they are represented in the text. Function $\Phi_{\delta}(E)$ is specified in Eqs. (10) (exact) and (13) (approximate); $\Phi_{\delta'}(E)$ is represented in Eq. (15), and its approximate expression is given by Eq. (19). Three upper graphs correspond to sls-band. In two lower graphs for WS-band, the rising and lowering lines represent $\Phi_{\delta}(E)$ and $\Phi_{\delta'}(E)$, respectively; $3\Phi_{\delta}^{\text{min}} = (\overline{eV}/2)^{3/2}$, $3\Phi_{\delta}^{\text{max}} = (\overline{eV})^{3/2}$. Functions $\Phi^{\pm} = \Phi_{\delta} \pm \Phi_{\delta'}$ are plotted by dotted lines.

Fig. 6. Transmission spectrum of WS-states assisted tunneling through the lowest miniband of a 51-well superlattice. Solid and dashed oscillating lines represent exact and approximate expressions of $T(E, \mathcal{E})$ given in Eqs. (2) and (16), respectively. Maxima envelope corresponds to Eq. (17) with $n\mathcal{E}$ replaced by E , and minima envelope corresponds to Eq. (18). In upper part $|A| = 0.1$; in the mid, $|A| = 1$; and for two lower graphs, $|A| = 100$.

Fig. 7. Tunneling probability above (or below) the tilted band, calculated from Eqs. (20) and (21) for different voltages (as indicated), is represented by solid and dashed lines, respectively. In calculations, $\mathcal{N} = 51$, $|A| = 0.1$.